International Journal of Refractory Metals and Hard Materials 125 (2024) 106887

Contents lists available at ScienceDirect

International Journal of Refractory Metals and Hard Materials

journal homepage: www.elsevier.com/locate/IJRMHM

Boriding of Ti-xNb alloys: Influence of Nb on the features of boride layer

Batuhan Sorusbay [a], Mertcan Kaba [b], Ferit Siyahcan [c], H. Ozkan Gulsoy [a], M. Suat Somer [c], Faiz Muhaffel [b], Huseyin Cimenoglu [b,*]

[a] Department of Metallurgical and Materials Engineering, Marmara University, 34722 Istanbul, Turkey
[b] Department of Metallurgical and Materials Engineering, Istanbul Technical University, 34469 Istanbul, Turkey
[c] Department of Chemistry, Koc University, 34450 Istanbul, Turkey

ARTICLE INFO

Keywords:
Ti—Nb alloys
Sintering
Boriding
Wear

ABSTRACT

In this study, Ti-xNb (x = 0–40 wt%) alloys produced by the powder metallurgy were borided with the aim of clarifying the effect of Nb on the structural and mechanical properties of the boride layer. After smearing the paste prepared from nano boron powder on the surfaces of the alloys, boriding was conducted at three different temperatures (900, 1000 and 1100 °C) for 8 h in a vacuum atmosphere. Unlike those formed at 900 °C, boriding temperatures of 1000 and 1100 °C provided thicker and homogenous boride layers. However, the boriding temperature of 1100 °C induced cracking within the boride layer of the Ti—40Nb alloy. For these reasons, the optimum boriding temperature was determined as 1000 °C. Increase in the Nb content not only increased the fraction of β-Ti phase in the microstructure of the sintered alloy at the expense of α-Ti, but also induced NbB_2 in the structure of the boride layer along with TiB_2. While Nb-poor α-Ti grains favoured the growth of TiB_2, TiB_2·NbB_2 mixture preferentially developed over the Nb-rich β-Ti grains. As the result of this, the hardness of the boride layer tended to decrease with increasing Nb content of the substrate. For example, the average hardness of the boride layers formed on Nb-free Ti and Ti—40Nb alloy were measured as ~2674 $HV_{0.025}$ and ~ 2460 $HV_{0.025}$, respectively. But regardless from the hardness, the boride layers provided a good protection for the underlying substrates against dry sliding contact and triggered abrasive wear on the contact surface of the counterface (WC-Co ball). The presence of NbB_2 in the boride layer led to a reduction in abrasive wear of the counterface. This finding revealed that in any wear-related application, where borided Ti alloys were intended to be used, it is better to choose high Nb-containing Ti alloys instead of α-Ti to minimize the wear of the tribo-couple via reducing the abrasion at the counter body.

1. Introduction

Titanium alloys, which are attractive engineering materials for aerospace, biomedical, defence and chemical industries, are classified as α, α + β and β alloys with respect to their room-temperature microstructure. In general, α alloys have good fracture toughness and corrosion resistance but limited mechanical properties, while α + β alloys have higher strength, ductility and low cycle fatigue strength. On the other hand, prominent properties of β alloys are low elastic modulus, high fatigue and excellent corrosion resistances [1–10].

However, Ti alloys do not exhibit sufficient performance when they are used in applications where high wear resistance is required. One of the technological solutions to this deficiency is application of surface treatment, among which boriding stands out [5,10–15]. As documented for many α and α + β alloys, boriding provides a remarkable enhancement in surface hardness and wear resistance upon formation of an external boride layer consisting of TiB_2 and/or TiB (Table 1). However, studies on the boriding of β alloys are scarce to the best knowledge of the authors. In a very limited number of studies conducted on β alloy (i.e. Ti—45Nb alloy) mainly the kinetics of boriding that favoured a boride layer composed of TiB_2 and NbB_2 (TiB_2·NbB_2 mixture) has been investigated by Kara and Purcek [11,16], without making any extra attempt to evaluate the effect of NbB_2 on the wear performance of the boride layer. This motivated the authors to conduct a systematic study to reveal the role of the phase structure of the boride layer on the wear resistance. Considering the β stabilizing effect of Nb, boriding studies were conducted on sintered Ti-xNb (x: 0–40 wt%) alloys, suggesting the possibility of increasing the NbB_2 content in the boride layer.

* Corresponding author.
E-mail addresses: batuhan.sorusbay@marmara.edu.tr (B. Sorusbay), mertcankaba@itu.edu.tr (M. Kaba), fsiyahcan@ku.edu.tr (F. Siyahcan), ogulsoy@marmara.edu.tr (H.O. Gulsoy), msomer@ku.edu.tr (M.S. Somer), muhaffel@itu.edu.tr (F. Muhaffel), cimenogluh@itu.edu.tr (H. Cimenoglu).

https://doi.org/10.1016/j.ijrmhm.2024.106887
Received 10 July 2024; Received in revised form 28 August 2024; Accepted 11 September 2024
Available online 12 September 2024

2. Materials and methods

2.1. Production of Ti-xNb alloys

This study has been conducted on Ti-xNb (x: 0–40 wt%) alloys produced by the powder metallurgy method. Spherical Ti and Nb powders (Alfa Aesar, 99.5 % purity, $\leq$ 45 μm) were used to prepare the alloys. Ti powder mixed with Nb powder at different ratios was milled in a planetary mill under an argon atmosphere for 1 h at a rotation speed of 350 rpm using 6 mm diameter balls at a 1:10 powder-to-weight ratio. The jars and balls used in the process were made of zirconia and the powder mixtures and balls were placed in the jar and sealed in a glovebox (MBraun) before the process. The powders were compacted in a 13 mm diameter mould under pressure of 370 MPa by using a uniaxial press (MSETM MP-0710). The green bodies were sintered in a tube furnace (Protherm PTF 17/75/300) in an argon atmosphere at 1400 °C for 1 h and then cooled to room temperature in the furnace.

2.2. Boriding process

Prior to paste boriding, the surfaces of the sintered samples were grinded and polished with a solution of 1 μm alumina and 0.25 μm colloidal silica (with 10 % H_2O_2) to achieve an average surface roughness (R_a) of ~0.25 μm. The boriding paste was prepared by mixing the nano boron powder (< 400 nm), obtained from Pavezyum Technical Ceramics company, with pure water. After smearing the paste to the surfaces, samples were immersed in boron powder and dried in an oven at 110 °C for 1 h. These samples were then placed in heat-resistant glass tubes and sealed in a vacuum (10^{-3} bar). The boriding process was carried out at 900, 1000 and 1100 °C for 8 h and cooling was done in the furnace (Protherm PLF 120/5).

2.3. Structural and mechanical characterisation

Structural characterisation of the samples was made via density measurements, phase analysis and microstructural examinations. Density measurements were carried out by using an Archimedes kit attached to precision balance (Precisa XB 320 M). Structural investigations were conducted on the cross-sections of the samples after grinding, polishing and etching with Kroll solution by using energy dispersive spectroscopy (EDS) equipped scanning electron microscopes (SEM, Hitachi TM-1000 and Jeol Neoscope JCM-7000). Phase analysis was made via X-ray diffraction (XRD) technique, where the samples were scanned in between 20 and 80° at 0.2° increments using a Cu-Kα tube with 28.5 mA and 35 kV power values on an X-ray diffractometer (GBC MMA 027).

The mechanical properties of the samples were determined by Vickers hardness (Wilson Tukon 1102), Rockwell-C adhesion (Zwick-Roell ZHR) and wear (Tribotech Oscillating Tribotester) tests. Vickers hardness measurements were carried out using 500 g of load on the surfaces of sintered samples and 25 g of load on the cross-sections of borided samples. The Rockwell-C adhesion tests were employed on the borided samples to determine the mechanical durability of the boride layers under a load of 150 kg. Circumferences of the Rockwell-C imprints were then examined with an optical microscope (OM, Nikon Eclipse L150) to survey the cracks that could have been developed. The wear tests of the samples were carried out at room temperature under dry reciprocating sliding contact condition. The counterface was chosen as 6 mm diameter WC-Co ball having hardness of ~1550 HV_1. The counterface ball's amplitude and sliding speed were 5 mm and 15 mm/s, respectively. While the wear tests of the sintered samples were made

Table 1
Examples of studies published since 2007 on the boriding of α and α + β alloys.

Alloy	Phase Structure	Boriding Method, Boron Source	Boriding Temperature, Boriding Time	Phase Structure and Thickness of boride Layer (~μm)	Ref.
CP-Ti (Grade 2)	α	Powder Pack Boriding, Amorphous Boron + Borax + Carbon	850–1050 °C 3–24 h	TiB_2 + TiB 23–54	[17]
Ti-6Al-4 V (Grade 23)	α + β	Pack Boriding, Ekabor II	1100 °C 2.5 h	TiB_2 + TiB 10	[12]
CP-Ti (Grade 2)	α	Powder Pack Boriding, Amorphous Boron + Borax + Carbon	850–1050 °C 3–24 h	TiB_2 + TiB 14.5–54	[18]
CP-Ti (Grade 2)	α	Electrochemical Boriding, Sodium Carbonate + Borax	900–1200 °C 0.16–4 h 50–700 mA/cm^2	TiB_2 + TiB 1.4–38.7	[19]
TC-21 (Ti-6Al-2Sn-2Zr-3Mo-1Cr-2Nb-0.09Si)	α + β	Powder Pack Boriding, Boron Carbide + Cerium Oxide	1000 °C 10 h	TiB_2 + TiB 43.4–44.7	[20]
CP-Ti (Grade 2)	α	Powder Pack Boriding, Boron Powder + Sodium Carbonate + Charcoal Activated	850–1050 °C 1–5 h	TiB_2 + TiB 2.5–4.52	[21]
CP-Ti (Grade 2)	α	Plasma Paste Boriding, Borax	700–800 °C 3–7 h	TiB_2 + TiB 1.9–6.3	[22]
Ti-6Al-4 V (Grade 5)	α + β	Plasma Paste Boriding, Borax	700–800 °C 3–7 h	TiB_2 + TiB 1.4–5.7	[23]
Ti-6Al-4 V (Grade 23)	α + β	Pack Boriding, Sodium Tetraborate + Boron Carbide + Potassium Chloride + Pure Aluminium	950–1100 °C 5–30 h	TiB_2 + TiB 8–28	[24]
CP-Ti (Grade 2)	α	Powder Pack Boriding, Amorphous Boron + Borax + Carbon	850–1200 °C 24 h	TiB_2 + TiB 39.3–23.8	[16]
Ti-6Al-4 V (Grade 23)	α + β			TiB_2 + TiB 12.5–21.1	
Ti-6Al-4 V (Grade 5)	α + β	Electrochemical Boriding, Borax + Sodium Carbonate	950 °C 0.5 h 500 mA/cm^2	TiB_2 55	[25]
CP-Ti (Grade 2)	α	Dissolved Salt Impregnation Technique, Aluminium + Borax	950–1150 °C 2 h	TiB_2 + TiB 17.4–64.9	[26]
Ti-6Al-4 V (Grade 5)	α + β	Pack Boriding, Sodium Tetraborate + Boron Carbide + Potassium Chloride + Pure Aluminium	850 °C 4–16 h	TiB_2 3.8–6.7	[27]

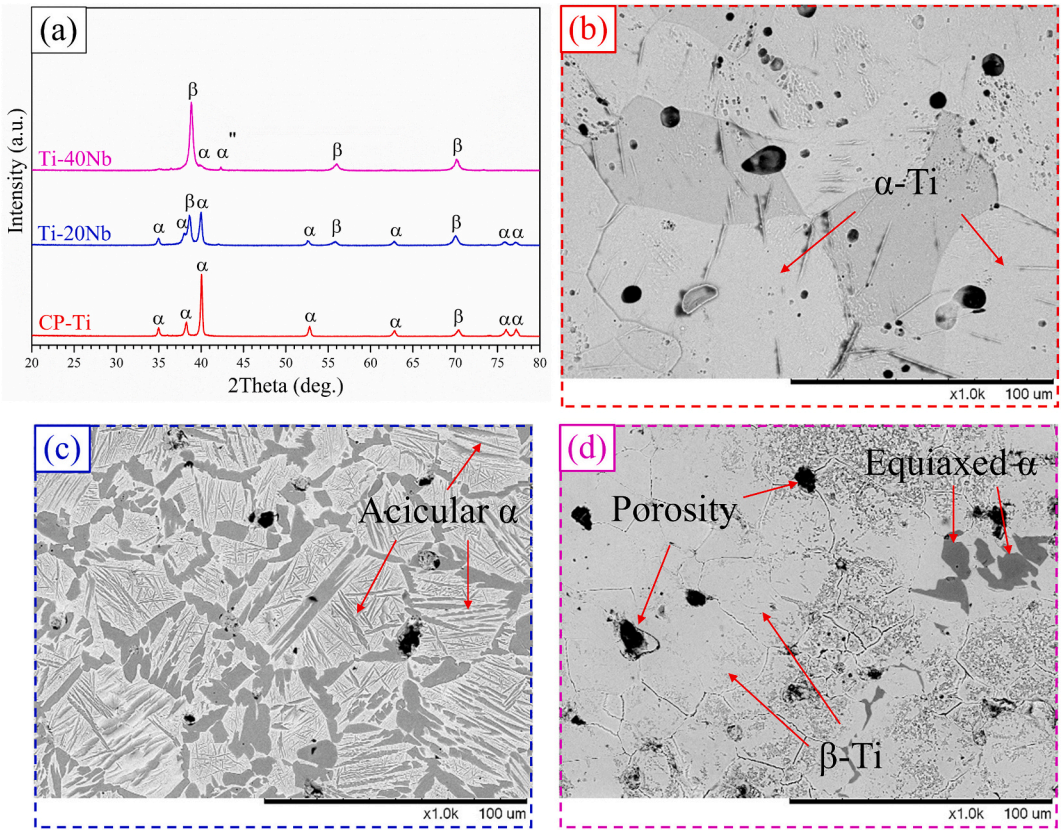

Fig. 1. (a) XRD patterns and SEM images of the sintered samples: (b) CP-Ti, (c) Ti—20Nb and (d) Ti—40Nb.

Table 2
Density, porosity, β-Ti fraction and hardness of the sintered alloys containing different amount of Nb.

Properties	CP-Ti	Ti-10Nb	Ti-20Nb	Ti-30Nb	Ti-40Nb
Density (g/cm^3)	4.32	4.52	4.74	4.92	5.06
Porosity (vol%)	4.16	7.90	10.84	14.03	17.49
β-Ti (vol%)	0	20.1	48.8	62.0	91.7
Hardness ($HV_{0.5}$)	412.1	376.1	328.6	268.7	221.1

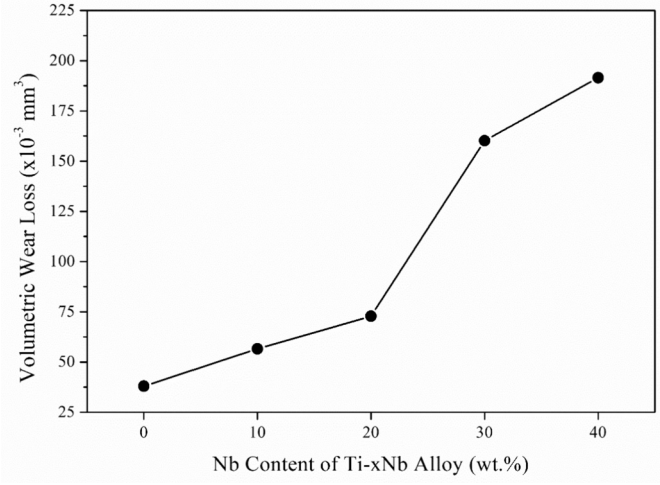

Fig. 2. The effect of Nb on the volumetric wear loss of the sintered Ti-xNb alloys. Wear tests were conducted under dry sliding contact condition by applying 1 N to the counterface (6 mm diameter WC-Co ball) for total sliding distance of 75 m.

under 1 N for a total sliding distance of 75 m, on the borided samples wear tests were conducted at a higher load and longer total sliding distance (i.e. 5 N and 225 m, respectively). After the wear tests, wear tracks formed on the samples were examined by using EDS equipped SEM (Thermo Scientific Axia ChemiSEM) and 2-D surface profilometer (Veeco Dectac 6 M). Also, the contact surface of the counterface balls were examined by OM.

3. Results and discussion

3.1. Structural characteristics and mechanical properties of the sintered samples

In Fig. 1, XRD patterns and SEM images of the sintered alloys are given for Nb-free, 20 and 40 wt% Nb containing alloys (hereafter will be referred as CP-Ti, Ti—20Nb and Ti—40Nb, respectively). No peaks other than hexagonal closed-packed (HCP) α-Ti were observed on the XRD pattern of the CP-Ti, but body-centered cubic (BCC) β-Ti peaks tend to appear gradually with the addition of Nb. While the intensities of α-Ti and β-Ti peaks were almost in the same range for the Ti—20Nb alloy, the peaks of β-Ti became more dominant for the Ti—40Nb alloy, at the expense of α-Ti peaks (Fig. 1a). SEM examinations confirmed the results of the XRD analysis so that according to Fig. 1 b-d, CP-Ti, Ti—20Nb and Ti—40Nb alloys can be classified as α, α + β and β alloys, respectively. While in the microstructure of CP-Ti and Ti—40Nb alloys, α-Ti and β-Ti grains appeared in equiaxed morphology, in the microstructure of the Ti—20Nb alloy, in addition to the network-like morphology surrounding the β-Ti grains, α-Ti also appeared in β-Ti grains in acicular morphology. It should be noted that in the microstructures of the examined alloys certain amount of porosities were also detected.

Density, porosity fraction, β-Ti fraction and hardness of the sintered alloys are given in Table 2 with respect to their Nb content. Due to the

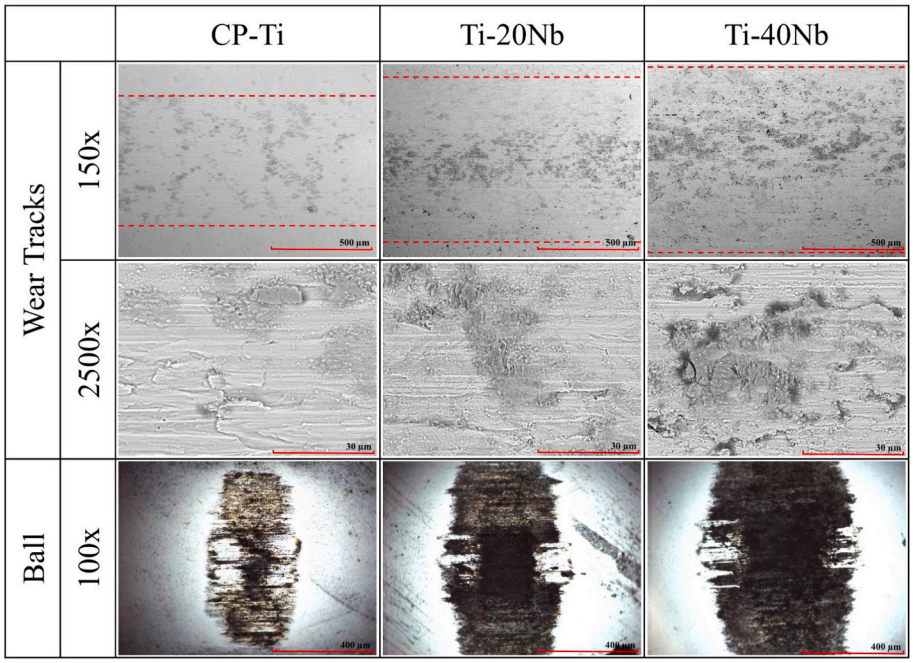

Fig. 3. SEM images of the wear tracks formed on sintered alloys and the OM images of wear scars formed on the relevant counterface WC-Co balls.

higher density of Nb compared to Ti, the addition of Nb increased the density of the sintered alloys along with an increase in porosity fraction, which was previously attributed to the slower diffusion rate of Nb compared to Ti during sintering [28,29]. Moreover, the addition of Nb led to a higher fraction of β-Ti in the microstructure and a reduction in hardness. Since BCC has higher slip systems than HCP, an increase in the volume fraction of β-Ti phase (BCC) in the microstructure at the expense of α-Ti (HCP) makes the Ti—Nb alloys more prone to plastic deformation, which results in a decrease in hardness [3].

The results of the sliding wear tests conducted on the sintered alloys under the load of 1 N for total sliding distance of 75 m are presented in Fig. 2 as a variation of the volumetric wear loss (calculated from the 2-D wear track profiles) with respect to the Nb content of the alloy. In good accordance with the domination of the β-Ti phase in the microstructure and reduction in hardness, wear loss increased with increasing Nb content of the alloy. In this regard, Ti—20Nb and Ti—40Nb alloys exhibited ~2 and ~ 5 times higher volumetric wear loss than CP-Ti, respectively.

SEM images of the wear tracks and OM images of the counterface ball are given in Fig. 3. As a general trend, domination of the β-Ti phase in the microstructure upon addition of Nb increased the severity of the adhesive wear as evidenced by increased intensity of delamination on the worn surface. Transfer of the material removed from the sintered alloys induced dark-colored wear scars on the counterface balls. In accordance with the widening of the wear track formed on sintered alloys, the wear scar of the counterface was enlarged when they got contact with higher Nb-containing alloys.

3.2. Structural characteristics and mechanical properties of the borided samples

In Fig. 4a, XRD patterns of the borided samples are presented. On the XRD pattern of the CP-Ti borided at 900 °C, α-Ti, TiB and TiB_2 peaks were detected. The increase of boriding temperature to 1000 and 1100 °C caused the disappearance of α-Ti and TiB peaks. On the XRD pattern of the Nb containing alloys in addition to the peaks of TiB_2, NbB_2 peaks also appeared. The intensity of the NbB_2 peaks tended to increase with increasing Nb content of the alloy and/or boriding temperature. However, β-Ti and TiB peaks appeared on the XRD pattern of the Ti—40Nb alloy borided at 1000 °C. It is worth noting that the detection of peaks of the substrate (α-Ti and β-Ti) on the XRD pattern of the borided alloys could be due to the penetration of X-rays beyond the boride layer.

Since 2θ of the most intense TiB_2 and NbB_2 peaks are very close to each other (44.44° and 43.46° respectively), the XRD patterns given in Fig. 4a are replotted in Fig. 4b for a narrower 2θ range (between 43° and 46°). It was noticed that the TiB_2 peak shifted to lower 2θ angles with increasing Nb content of the substrate. According to standard JCPDS database, while the 2θ angle corresponding to the TiB_2 peak (44.44°, JCPDS 35–0741) in CP-Ti is completely consistent, the TiB_2 peak of the borided Ti—40Nb alloy appeared at 2θ angle of 44.07° by getting closer to the 2θ angle of NbB_2 peak (43.46°, JCPDS 35–0742). The shifting of the TiB_2 peak towards the NbB_2 peak with increasing Nb content of the substrate can be associated with lattice distortion arising from the replacement of Ti atoms with larger Nb atoms in the TiB_2 crystal lattice. Considering this fact, Kara and Purcek [11] defined the phase structure of the boride layer formed over commercial β type Ti—45Nb alloy as $TiB_2{\cdot}NbB_2$ mixture. After pack boriding of Ti-46.6Al, Ti-45.2Al-7.2Nb and Ti-44.8Al-6.6Ta alloys, Popela and Vojtěch [30] detected similar peak shift on the XRD pattern in the presence of Nb and Ta in Ti—Al alloy. They also correlated this observation with formation of mixed borides ($TiB_2{\cdot}NbB_2$ and $TiB_2{\cdot}TaB_2$) within the boride layer, which exposed to lattice expansion upon replacement of Ti by Nb and Ta.

High magnification SEM examination (Fig. 5) conducted on the Ti—40Nb alloy borided at 1100 °C confirmed that $TiB_2{\cdot}NbB_2$ preferentially forms over the bright-coloured Nb-rich β-Ti grains, while dark-colored Nb-poor α-Ti grains favour the formation of TiB_2. In Fig. 6 the results of the EDS line scan analysis are depicted for Ti—20Nb alloy borided at 1100 °C. Horizontal and vertical line scan EDS analysis (Line 1 and Line 2) revealed that higher concentration of Nb was detected at the brighter regions, while darker region was rich in Ti. This observation is in accordance with more intense presence of NbB_2 in brighter regions of the boride layer.

Low-magnification cross-sectional SEM images of the CP-Ti,

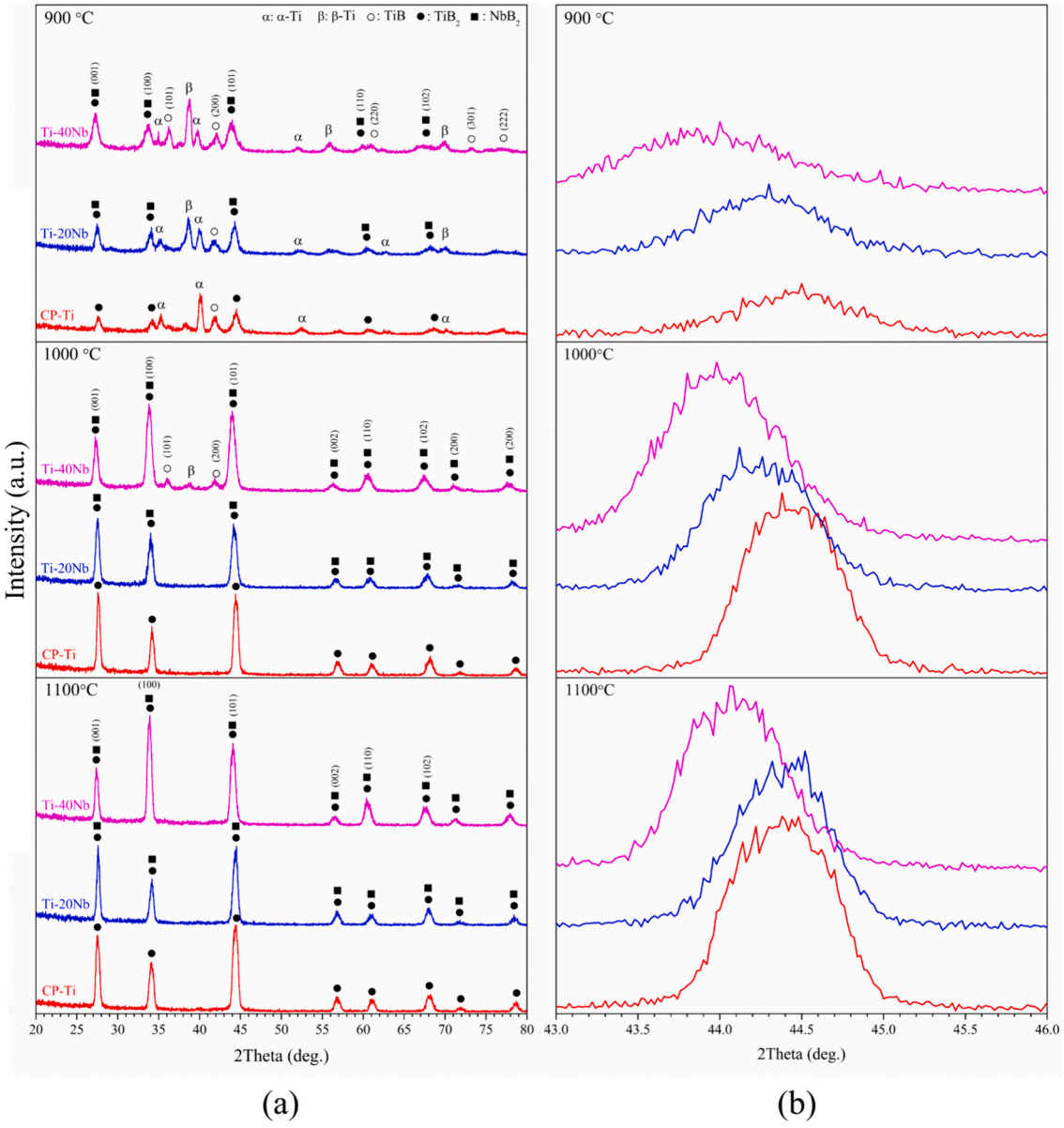

Fig. 4. XRD patterns of the borided CP-Ti, Ti—20Nb and Ti—40Nb alloys for wide and narrow scanning angles of (a) 20–80 and (b) 43–46, respectively.

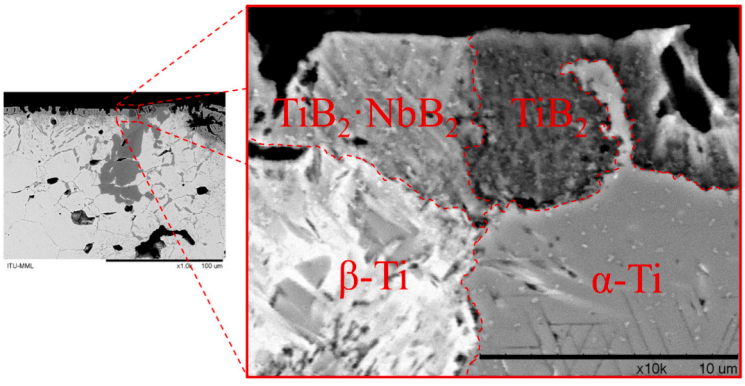

$TiB_2 \cdot NbB_2$

Element	Atomic %	Weight %
B	60.00	22.78
Ti	33.72	56.72
Nb	6.28	20.50

TiB_2

Element	Atomic %	Weight %
B	63.17	27.79
Ti	36.59	71.3
Nb	0.91	0.24

Fig. 5. Cross-sectional SEM images and point EDS results of the borides grown on α- and β-Ti grains. This image was taken from the Ti—40Nb alloy borided at 1100 °C.

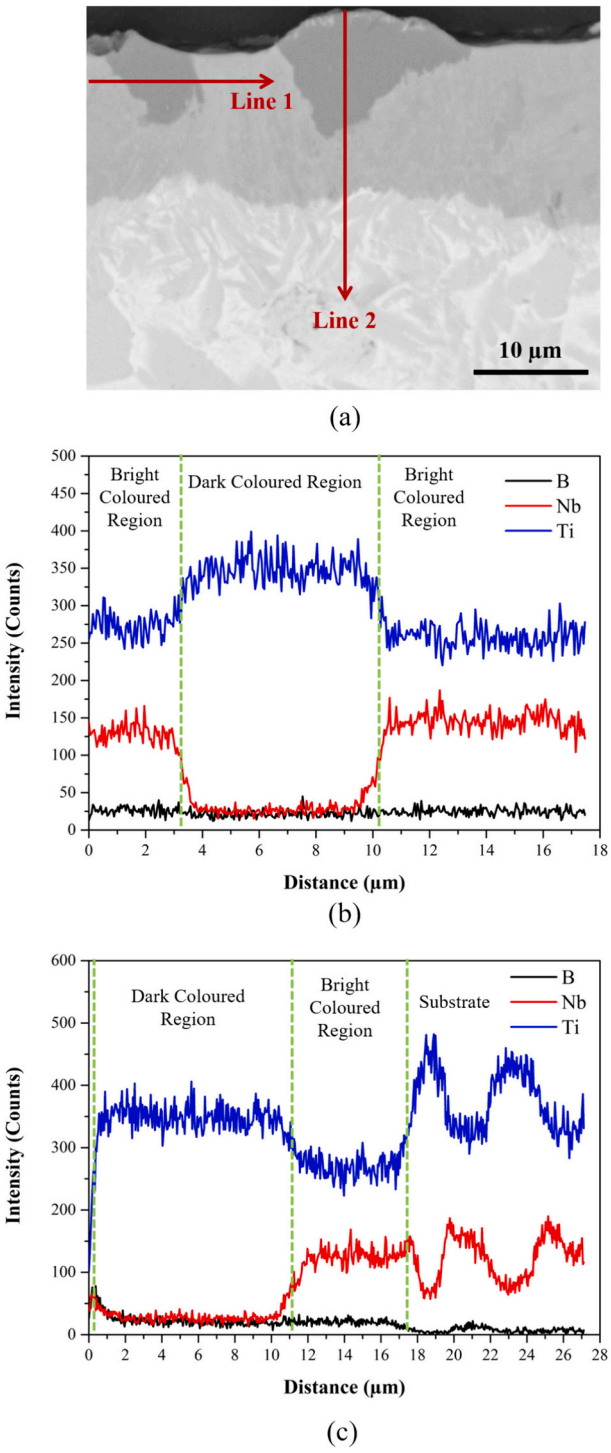

Fig. 6. (a) Cross-sectional SEM image of the Ti—20Nb alloy borided at 1100 °C and results of EDS line analysis showing distribution of Ti, Nb and B along (b) Line 1 and (c) Line 2.

Ti—20Nb and Ti—40Nb alloys borided at three different temperatures are shown in Fig. 7. Boriding at 900 °C produced a thin and discontinuous boride layer. Increasing the boriding temperature to 1000 °C formed a distinct and continuous boride layer. The boriding temperature of 1100 °C favoured a further increase in the thickness of the boride layer. However, microcracks were detected within the boride layer of Ti—40Nb alloy borided at 1100 °C. When the difference in the thermal expansion coefficients of TiB_2, NbB_2 and the underlying β-Ti phases (~4.6 × 10^{-6}/°C [11], ~8 × 10^{-6}/°C [11] and ~ 27.9 × 10^{-6}/°C [31], respectively) is taken into consideration, it is suggested that development of large thermal stresses during boriding played a crucial role on cracking of the boride layer (especially at higher boriding temperatures and Nb content of the substrate).

The boride layer thicknesses of the examined Ti-xNb alloys are presented in Fig. 8 for different boriding temperatures. Boriding temperatures of 1000 and 1100 °C, provided thicker boride layers. When the Nb contents of the sintered alloys are taken into consideration, the thickness of the boride layer tends to decrease after reaching a max value at a certain Nb content. The maximum boride layer thicknesses were measured as ~9.0 µm for the boriding temperature of 1000 °C and ~ 13.5 µm for the boriding temperature of 1100 °C on the Ti—10Nb and Ti—20Nb alloys, respectively. The initial increase in the boride layer thickness with Nb content of the substrate can be explained by acceleration of boron diffusion with increasing the number of mixed boride (TiB_2·NbB_2) interfaces [30]. Reduction in the boride layer thickness with further increase in the Nb content is suggested to be arisen from the thermal expansion coefficient mismatch (between TiB_2, NbB_2 and substrate) leading cracking induced local detachment from boride layer (Fig. 7).

The results of the hardness measurements conducted on the cross-sections of the boride layers are depicted in Fig. 9. As a general trend, boride layer hardness decreased with increasing Nb content of the substrate. After the Rockwell-C adhesion tests conducted on the borided surfaces, no delamination or fragmentation was observed in the vicinity of the Rockwell-C indents except from the cracks (Fig. 10). The severity of boride layer cracking tended to decrease with increasing Nb content of the substrate. Finally, it was determined that the boride layers formed on the examined Ti-xNb alloys were in the HF1 category of the Daimler-Benz Rockwell-C adhesion test chart [32].

Based on these findings, the decrease in the hardness (Fig. 9) and cracking tendency (Fig. 10) of the boride layers with an increase in the Nb content of the substrate can be attributed to the larger participation of NbB_2 into the boride layer, having lower hardness but higher fracture toughness compared to TiB_2. In the literature, the hardness and the fracture toughness of the TiB_2 and NbB_2 were reported as ~31.7 GPa, ~3.4 MPa·$m^{1/2}$ and ~ 20 GPa, ~3.8 MPa·$m^{1/2}$, respectively [33,34].

As the examples of the dry sliding wear test results conducted on the borided Ti-xNb alloys against WC-Co balls under 5 N load for the sliding distance of 225 m, SEM images and EDS elemental mapping of the wear tracks are presented for the CP-Ti and Ti—40Nb alloys in Fig. 11. In general, the rubbing action of the counterface ball caused smoothening of the boride layer and did not induce cracking and delamination. Despite a decrease in the width of the wear track with increasing Nb content of the substrate, the depths of the wear tracks were not measurable by a profilometer. EDS elemental mapping revealed that the white-coloured regions detected in the wear tracks were rich in W, C, Co and O, while compositional elements of the boride layers (Ti, Nb and B) were identified in other regions. It is worth noting that the intensity of the white-coloured regions tended to decrease with increasing Nb content of the substrate. In accordance with this observation, evidences of abrasive wear were identified on the contact surfaces of the counterface WC-Co balls having a hardness (~1550 HV_1) lower than those of the boride layers (Fig. 9). Thus, sliding contact with the boride layers induced grooves aligned in the sliding direction within the wear scars of the counterface balls (Fig. 12). The decrease of the wear scar size of the counterface ball and the narrowing of the wear track formed on the boride layer with increasing Nb content of the substrate can be attributed to the reduction of the boride layer hardness (Fig. 9). This led a decrease in the abrasive effect of the boride layer on the counterface. For this reason, on the wear track of the borided Ti—40Nb alloy limited amount of material transfer from the counterface WC-Co ball, as evidenced by low fraction of W, C, Co and O enriched white coloured region, was detected compared to the borided CP-Ti (Fig. 11). From the perspective of minimizing the wear of the tribo-couple, it can

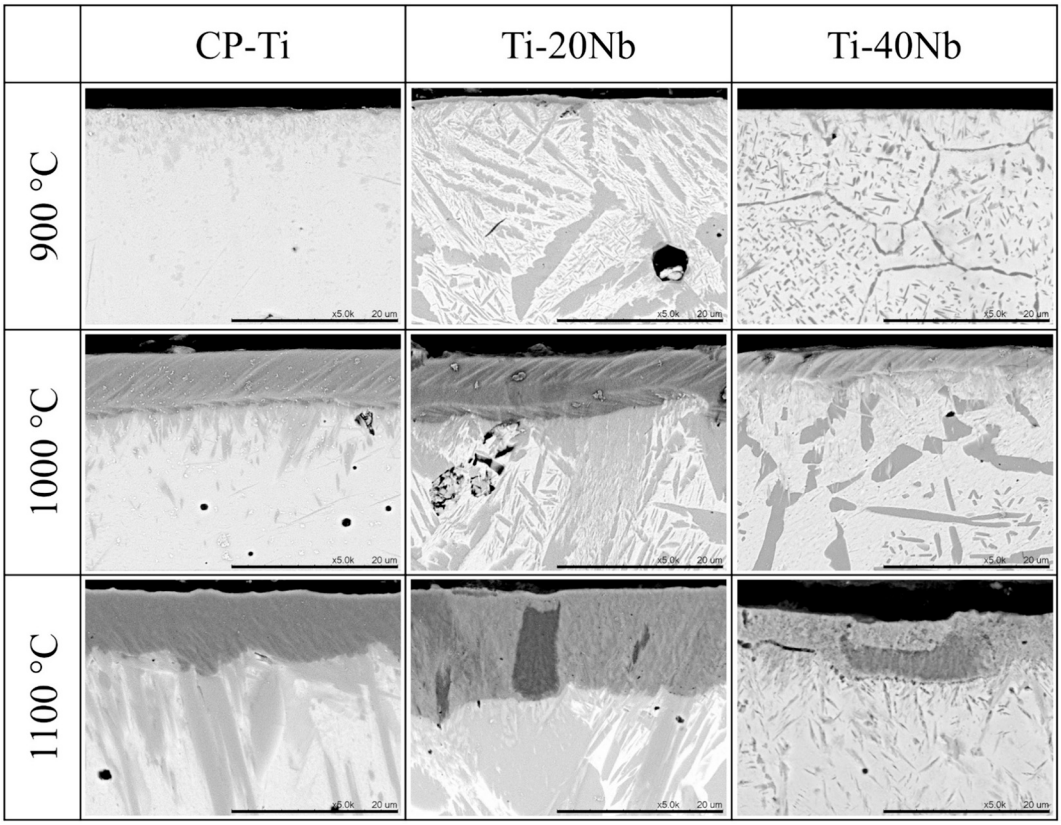

Fig. 7. Cross-sectional SEM images of CP-Ti, Ti—20Nb and Ti—40Nb samples borided at different temperatures.

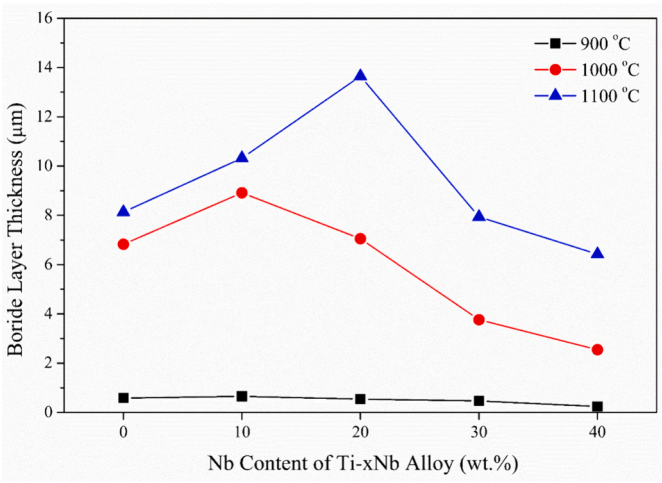

Fig. 8. The effect of Nb content of the Ti-xNb alloy on the boride layer thickness.

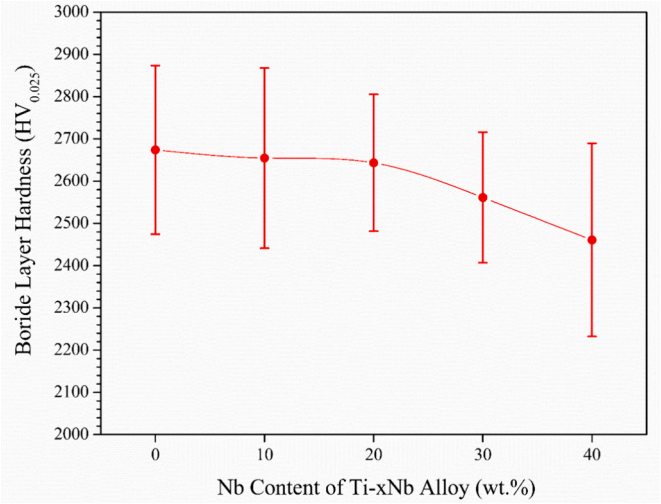

Fig. 9. The effect of Nb content of the Ti-xNb alloy on the boride layer hardness.

confidently be expressed that the higher the Nb content of the substrate, the longer will be service life of the boride layer/counterface contact.

4. Conclusions

In this study, Ti-xNb (x = 0–40 wt%) alloys sintered at 1400 °C were borided by the paste boriding technique using nano boron powder at temperatures of 900, 1000 and 1100 °C. The results of the structural examination and mechanical test conducted on the as-sintered and borided alloys are summarised below.

Sintered Alloys:

- Compared to the sintered CP-Ti, having a microstructure composed entirely of α-Ti, Nb addition favoured the formation of β-Ti in the microstructure. In the microstructures of Ti—20Nb and Ti—40Nb alloy, the volume fraction of the β-Ti were ~ 49 % and ~ 92 %, respectively. The increase in Nb content of the alloy resulted in larger porosity volume fraction up to ~18 %.
- Domination of β-Ti in the microstructure was accompanied by a reduction in hardness. While the hardness of the CP-Ti was ~412 $HV_{0.5}$, the hardnesses of Ti—20Nb and Ti—40Nb alloys measured as ~328 $HV_{0.5}$ and ~ 221 $HV_{0.5}$, respectively.

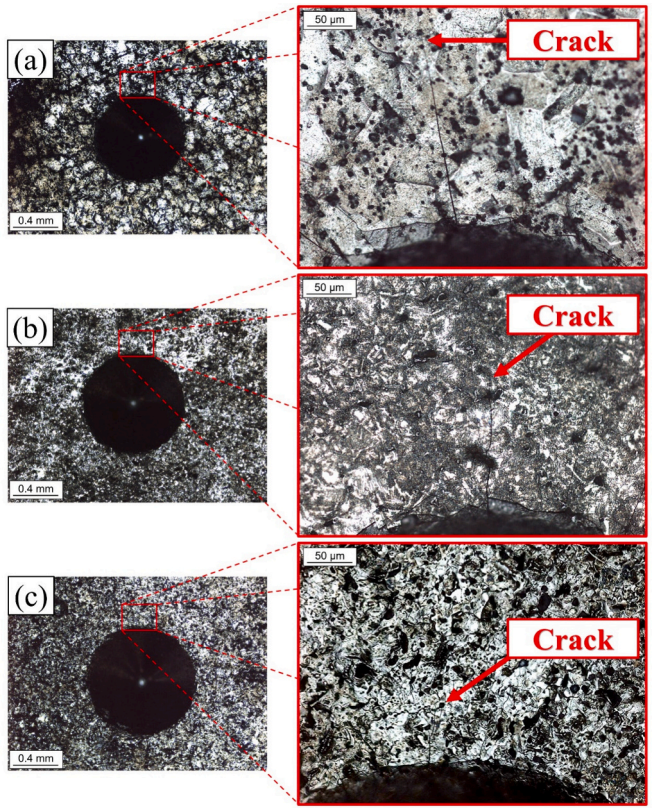

Fig. 10. OM images of the indents and their vicinity formed on the boride layers of (a) CP-Ti, (b) Ti—20Nb and (c) Ti—40Nb alloys.

- Under dry sliding contact, Ti-xNb alloys were worn by adhesive wear mechanism, where the severity of adhesive wear increased with increasing Nb content of the alloy. In this regard, Ti—20Nb and Ti—40Nb alloys exhibited ~2 and ~ 5 times higher wear rates than CP-Ti, respectively.

Borided Alloys:

- The paste prepared in this study by using nano boron powder successfully borided the sintered Ti-xNb alloys at ≥1000 °C. However, the boriding temperature of 1100 °C induced cracking in the boride layer as the Nb content of the substrate increased (especially for the Ti—40Nb alloy).
- Boriding at 1000 °C produced a boride layer consisting of TiB_2 with a thickness of ~6.82 µm on CP-Ti and the ~2.55 µm thick boride layer consisting of TiB_2·NbB_2 over the Ti—40Nb alloy. In Ti-xNb alloys, TiB_2 grows on the Nb-poor α-Ti grains and TiB_2·NbB_2 mixture grows on Nb-rich β-Ti grains.
- The presence of NbB_2 in the boride layer, reduces the hardness. While the hardness of the boride layer formed on the CP-Ti sample was 2674 $HV_{0.025}$, the hardness of the boride layer of the Ti—40Nb alloy was measured as 2460 $HV_{0.025}$. Nevertheless, boride layers formed on the examined Ti-xNb alloys were in the HF1 category of the Daimler-Benz Rockwell-C adhesion test chart, increase in NbB_2 in the boride layer restricted the formation of cracks around the Rockwell-C indents as the indication of increase in toughness.
- After the dry sliding wear tests performed under a 5 N load by using 6 mm diameter WC-Co balls, no significant wear loss was quantified on the boride layers. During the test, the boride layers were subjected to the polishing effect by the counter balls, while the counter balls were worn by abrasion.

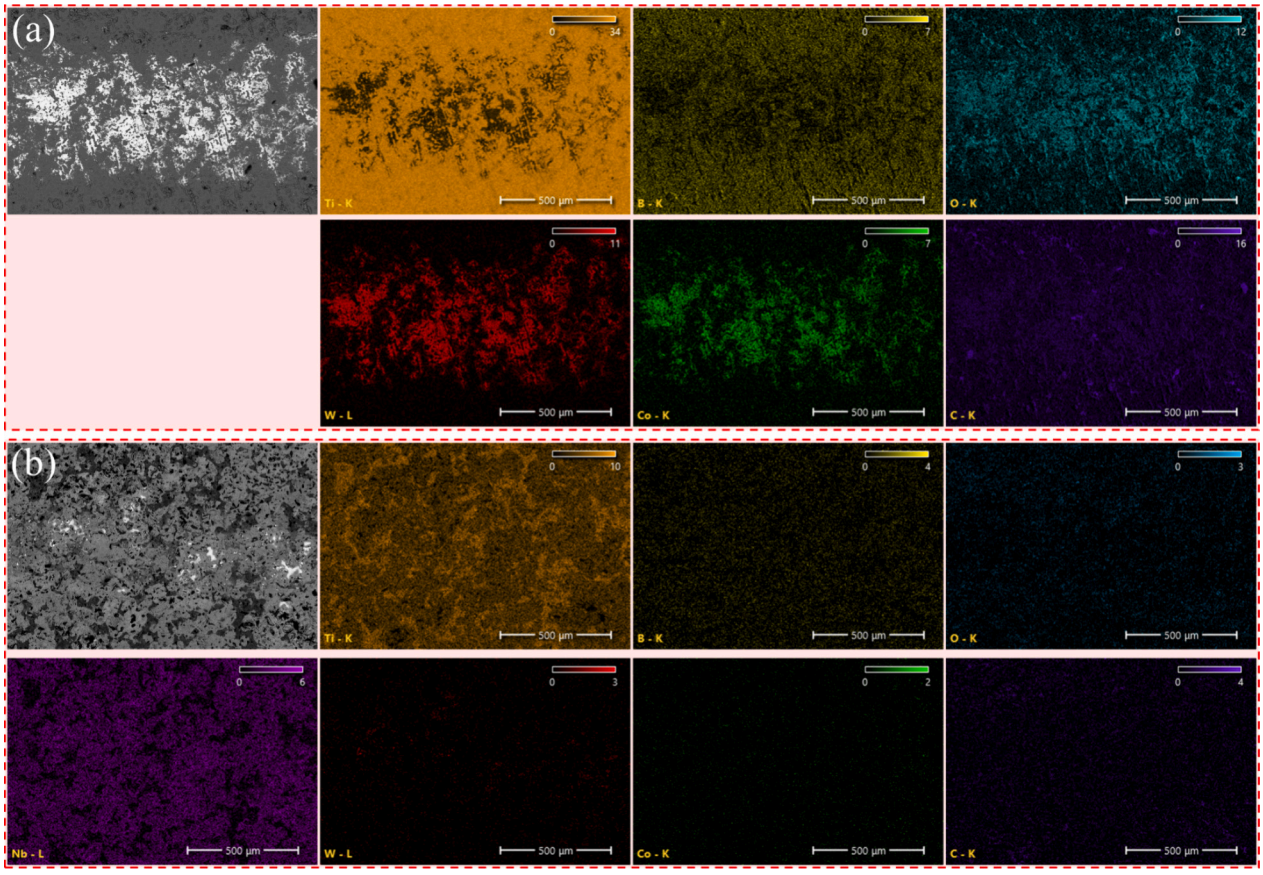

Fig. 11. SEM and elemental EDS mapping images taken from wear tracks of the borided (a) CP-Ti and (b) Ti—40Nb alloys worn under dry sliding contact conditions by applying 5 N to the 6 mm diameter WC-Co ball for a total sliding distance of 225 m.

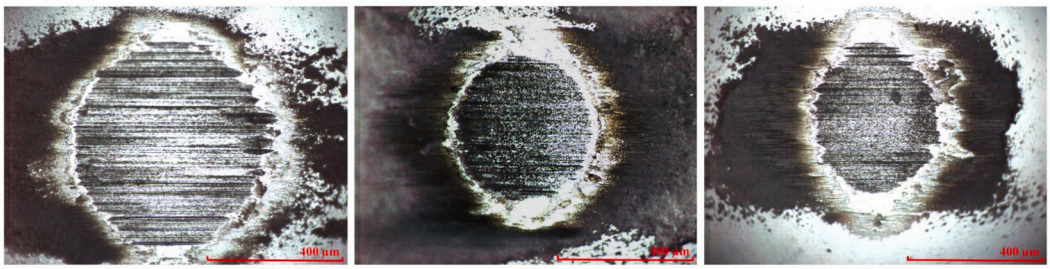

Fig. 12. OM images of wear scars formed on counterface balls used in wear tests conducted on borided (a) CP-Ti, (b) Ti—20Nb and (c) Ti—40Nb alloys.

- The wear loss of the borided Ti-xNb alloy/WC-Co ball tribo-couple decreased with increasing Nb content of the substrate, which caused the counterface to expose less abrasion.

Statement of originality

The submitted article titled "Boriding of Ti-xNb Alloys: Influence of Nb on the Features of Boride Layer" was prepared by the M.Sc. thesis of Mr. B. Sorusbay. The article is entirely original and has not been published or is under consideration for publication elsewhere.

CRediT authorship contribution statement

Batuhan Sorusbay: Writing – original draft, Investigation, Formal analysis. **Mertcan Kaba:** Investigation, Formal analysis. **Ferit Siyahcan:** Resources, Investigation. **H. Ozkan Gulsoy:** Investigation. **M. Suat Somer:** Resources. **Faiz Muhaffel:** Writing – review & editing, Investigation, Formal analysis. **Huseyin Cimenoglu:** Writing – review & editing, Supervision, Resources, Conceptualization.

Declaration of competing interest

The authors declare that they have no known competing financial interests or personal relationships that could have appeared to influence the work reported in this paper.

Data availability

Data will be made available on request.

Acknowledgements

This study was funded by Istanbul Technical University (ITU) through ITU-BAP MYL-2021-43150 project. The authors would like to express their acknowledgements to ITU Solak Group and Karfo Endüstriyel Co. for EDS-SEM investigations and ITU Particulate Materials Laboratories for milling and pressing of the powder mixtures.

References

[1] J. Ruan, H. Yang, X. Weng, J. Miao, K. Zhou, Preparation and characterization of biomedical highly porous Ti–Nb alloy, J. Mater. Sci. Mater. Med. 27 (2016) 76, https://doi.org/10.1007/s10856-016-5685-6.
[2] A.M.G. Tavares, W.S. Ramos, J.C.G. de Blas, E.S.N. Lopes, R. Caram, W.W. Batista, S.A. Souza, Influence of Si addition on the microstructure and mechanical properties of Ti–35Nb alloy for applications in orthopedic implants, J. Mech. Behav. Biomed. Mater. 51 (2015) 74–87, https://doi.org/10.1016/j.jmbbm.2015.06.035.
[3] M. Peters, J. Hemptenmacher, J. Kumpfert, C. Leyens, Structure and properties of titanium and titanium alloys, in: C. Leyens, M. Peters (Eds.), Titanium and Titanium Alloys, Wiley-VCH Verlag GmbH & Co. KGaA, Weinheim, FRG, 2005, pp. 1–36, https://doi.org/10.1002/3527602119.ch1.
[4] G. Lütjering, J.C. Williams, Titanium, 2nd ed, Springer, Berlin, Heidelberg, 2007, https://doi.org/10.1007/978-3-540-73036-1.
[5] P. Li, D. Liu, W. Bao, L. Ma, Y. Duan, Surface characterization and diffusion model of pack borided TB2 titanium alloy, Ceram. Int. 44 (2018) 18429–18437, https://doi.org/10.1016/j.ceramint.2018.07.060.
[6] S. Liang, Review of the Design of Titanium Alloys with low elastic Modulus as implant materials, Adv. Eng. Mater. 22 (2020) 2000555, https://doi.org/10.1002/adem.202000555.
[7] J. Lin, Y. Zhang, M. Ma, Preparation of porous Ti35Nb alloy and its mechanical properties under monotonic and cyclic loading, Trans. Nonferrous Metals Soc. China 20 (2010) 390–394, https://doi.org/10.1016/S1003-6326(09)60151-5.
[8] H. Huang, P.-H. Lan, Y.-Q. Zhang, X.-K. Li, X. Zhang, C.-F. Yuan, X.-B. Zheng, Z. Guo, Surface characterization and in vivo performance of plasma-sprayed hydroxyapatite-coated porous Ti6Al4V implants generated by electron beam melting, Surf. Coat. Technol. 283 (2015) 80–88, https://doi.org/10.1016/j.surfcoat.2015.10.047.
[9] S.N. Dahotre, H.D. Vora, K. Pavani, R. Banerjee, An integrated experimental and computational approach to laser surface nitriding of Ti–6Al–4V, Appl. Surf. Sci. 271 (2013) 141–148, https://doi.org/10.1016/j.apsusc.2013.01.151.
[10] M. Geetha, A.K. Singh, R. Asokamani, A.K. Gogia, Ti based biomaterials, the ultimate choice for orthopaedic implants – a review, Prog. Mater. Sci. 54 (2009) 397–425, https://doi.org/10.1016/j.pmatsci.2008.06.004.
[11] G. Kara, G. Purcek, Growth kinetics and mechanical characterization of boride layers formed onβ-type Ti-45Nb alloy, Surf. Coat. Technol. 352 (2018) 201–212, https://doi.org/10.1016/j.surfcoat.2018.07.085.
[12] E. Atar, E.S. Kayali, H. Cimenoglu, Characteristics and wear performance of borided Ti6Al4V alloy, Surf. Coat. Technol. 202 (2008) 4583–4590, https://doi.org/10.1016/j.surfcoat.2008.03.011.
[13] Y.L. Zhou, M. Niinomi, T. Akahori, Effects of ta content on Young's modulus and tensile properties of binary Ti–ta alloys for biomedical applications, Mater. Sci. Eng. A 371 (2004) 283–290, https://doi.org/10.1016/j.msea.2003.12.011.
[14] M. Long, H.J. Rack, Friction and surface behavior of selected titanium alloys during reciprocating-sliding motion, Wear 249 (2001) 157–167, https://doi.org/10.1016/S0043-1648(01)00517-8.
[15] J. Probst, U. Gbureck, R. Thull, Binary nitride and oxynitride PVD coatings on titanium for biomedical applications, Surf. Coat. Technol. 148 (2001) 226–233, https://doi.org/10.1016/S0257-8972(01)01357-3.
[16] G. Kara, G. Purcek, Boriding behaviour of titanium alloys with different crystalline structures, Surf. Eng. 35 (2019) 611–617, https://doi.org/10.1080/02670844.2018.1552646.
[17] N.M. Tikekar, K.S. Ravi Chandran, A. Sanders, Nature of growth of dual titanium boride layers with nanostructured titanium boride whiskers on the surface of titanium, Scr. Mater. 57 (2007) 273–276, https://doi.org/10.1016/j.scriptamat.2007.03.050.
[18] B. Sarma, N.M. Tikekar, K.S. Ravi Chandran, Kinetics of growth of superhard boride layers during solid state diffusion of boron into titanium, Ceram. Int. 38 (2012) 6795–6805, https://doi.org/10.1016/j.ceramint.2012.05.077.
[19] A. Kilic, G. Kartal, M. Urgen, S. Timur, Effects of electrochemical boriding process parameters on the formation of titanium borides, Surf. Eng. Appl. Electrochem. 49 (2013) 168–175, https://doi.org/10.3103/S1068375513020051.
[20] Y.S. Zhu, W.Z. Lu, D.W. Zuo, W. Feng, Y.F. He, Microstructure and tribological properties of REs borided TC21 alloy, Surf. Eng. 30 (2014) 612–618, https://doi.org/10.1179/1743294414Y.0000000292.
[21] B. Sivakumar, R. Singh, L.C. Pathak, Corrosion behavior of titanium boride composite coating fabricated on commercially pure titanium in Ringer's solution for bioimplant applications, Mater. Sci. Eng. C 48 (2015) 243–255, https://doi.org/10.1016/j.msec.2014.12.002.
[22] M. Keddam, S. Taktak, S. Tasgetiren, A diffusion model for the titanium borides on pure titanium, Surf. Eng. 32 (2016) 802–808, https://doi.org/10.1080/02670844.2016.1180845.
[23] M. Keddam, S. Taktak, Characterization and diffusion model for the titanium boride layers formed on the Ti6Al4V alloy by plasma paste boriding, Appl. Surf. Sci. 399 (2017) 229–236, https://doi.org/10.1016/j.apsusc.2016.11.227.
[24] Y. Duan, P. Li, Z. Chen, J. Shi, L. Ma, Surface evolution and growth kinetics of Ti6Al4V alloy in pack boriding, J. Alloys Compd. 742 (2018) 690–701, https://doi.org/10.1016/j.jallcom.2018.01.383.
[25] A. Kaouka, K. Benarous, Electrochemical boriding of titanium alloy Ti-6Al-4V, J. Mater. Res. Technol. 8 (2019) 6407–6412, https://doi.org/10.1016/j.jmrt.2019.10.024.

[26] T. Chen, S. Koyama, L. Yu, Improvement of mechanical, Tribological, and fricative reduction properties of pure titanium by Boriding, Appl. Sci. 11 (2021) 4862, https://doi.org/10.3390/app11114862.
[27] B. Rahmatian, H.M. Ghasemi, M. Heydarzadeh Sohi, P. De Baets, Tribocorrosion and corrosion behavior of double borided layers formed on Ti-6Al-4V alloy: an approach for applications to bio-implants, Corros. Sci. 210 (2023) 110824, https://doi.org/10.1016/j.corsci.2022.110824.
[28] D. Zhao, K. Chang, T. Ebel, H. Nie, R. Willumeit, F. Pyczak, Sintering behavior and mechanical properties of a metal injection molded Ti–Nb binary alloy as biomaterial, J. Alloys Compd. 640 (2015) 393–400, https://doi.org/10.1016/j.jallcom.2015.04.039.
[29] Y. Chen, P. Han, A. Dehghan-Manshadi, D. Kent, S. Ehtemam-Haghighi, C. Jowers, M. Bermingham, T. Li, J. Cooper-White, M.S. Dargusch, Sintering and biocompatibility of blended elemental Ti-xNb alloys, J. Mech. Behav. Biomed. Mater. 104 (2020) 103691, https://doi.org/10.1016/j.jmbbm.2020.103691.
[30] T. Popela, D. Vojtěch, Characterization of pack-borided last-generation TiAl intermetallics, Surf. Coat. Technol. 209 (2012) 90–96, https://doi.org/10.1016/j.surfcoat.2012.08.034.
[31] M. Bönisch, A. Panigrahi, M. Stoica, M. Calin, E. Ahrens, M. Zehetbauer, W. Skrotzki, J. Eckert, Giant thermal expansion and α-precipitation pathways in Ti-alloys, Nat. Commun. 8 (2017) 1429, https://doi.org/10.1038/s41467-017-01578-1.
[32] N. Vidakis, A. Antoniadis, N. Bilalis, The VDI 3198 indentation test evaluation of a reliable qualitative control for layered compounds, J. Mater. Process. Technol. 143–144 (2003) 481–485, https://doi.org/10.1016/S0924-0136(03)00300-5.
[33] I. Akin, B.C. Ocak, F. Sahin, G. Goller, Effects of *SiC* and *SiC* -GNP additions on the mechanical properties and oxidation behavior of NbB_2, J. Asian Ceram. Soc. 7 (2019) 170–182, https://doi.org/10.1080/21870764.2019.1595929.
[34] N.S. Karthiselva, B.S. Murty, S.R. Bakshi, Low temperature synthesis of dense TiB2 compacts by reaction spark plasma sintering, Int. J. Refract. Met. Hard Mater. 48 (2015) 201–210, https://doi.org/10.1016/j.ijrmhm.2014.09.015.